Detecting and mapping a CO_2 plume with novel autonomous pH sensors on an underwater vehicle

Samuel A. Monk [a,b,*], Allison Schaap [a], Rudolf Hanz [a], Sergey M. Borisov [c], Socratis Loucaides [a], Martin Arundell [a], Stathys Papadimitriou [a], John Walk [a], Daisy Tong [a], James Wyatt [a], Matthew Mowlem [a,b]

[a] Waterfront Campus, European Way, NOC National Oceanography Centre, Southampton SO14 3ZH, UK
[b] Presently also at ClearWater Sensors Ltd., UK
[c] Institute of Analytical Chemistry and Food Chemistry, Graz University of Technology, Stremayrgasse 9, Graz 8010, Austria

ABSTRACT

We report the first successful use of chemical sensors integrated on to an underwater vehicle to locate, map and estimate flux from a controlled sub-seabed CO_2 release, analogous to a leak from a Carbon Capture and Storage (CCS) reservoir. This has global implications for the efficacy and cost of monitoring of offshore CCS sites and hence public and regulatory confidence as this tool for addressing climate change is considered and rolled out. A remotely operated vehicle (ROV) equipped with three different pH sensors was deployed to determine the spatial extent of the controlled release. The sensors each operated on a different principle (spectrophotometric, fluorescence, and electrochemical) and the strengths and weaknesses of each sensor are discussed. The sensor data demonstrated that evidence of the plume was limited to within 3 m of the seafloor, as predicted by previous modelling work. The data were then utilised to develop a model of the plume, to extend the spatial coverage of the data. This comparison of the three sensors and the insight into plume dynamics provided by the model would assist in the planning of future plume surveys to ensure the sensor and vehicle combination can resolve the plume of interest.

1. Introduction

Reduced greenhouse gas emissions alone are unlikely to be enough to reach the target of keeping global temperatures within 2 °C of preindustrial levels, as is the aim of current policies set by the Paris agreement (UNFCCC. Conference of the Parties (COP), 2015). Carbon capture and storage (CCS) has the potential to become an increasingly important mitigation technique (Mac Dowell et al., 2017). The principle behind CCS is that CO_2 is captured, most likely at point sources such as power plants, cement factories or oil refineries, and is stored in geological formations isolated from the atmosphere rather than being released (IPCC, 2005; Schrag, 2009). Depleted oil and gas reservoirs have been suggested as storage sites, as their geology is well suited to trapping fluids (Schrag, 2009). Prior to offshore CCS becoming a viable, widely accepted and adopted method its potential impacts need to be understood (Blackford et al., 2015, 2014; Dixon and Romanak, 2015; Wallmann et al., 2015). A leak from an offshore CCS site would not only

return the CO_2 removed to the atmosphere but would also alter seawater chemistry with potential impacts on the marine environment. To address this, in the last decade three experiments have been conducted to study the potential impact of leaks from a subsea reservoir (Blackford et al., 2014; Dean and Tucker, 2017; Flohr et al., 2021). A review of these experiments highlighted not only the need to monitor sites, in order to identify and quantify potential leaks, but also to have a plan in place on how to address them (Dean et al., 2020).

The detection of a chemical plume is a challenge in the ocean. Complex circulation patterns operating over potentially large spatial extents combined with high background spatiotemporal variability all contribute to the difficulty (Alendal, 2017). Plume features are not unique to CCS leaks, and there are several analogues, both natural and anthropogenic. Natural chemical plumes include natural gas seeps (Gros et al., 2019; Schmidt et al., 2014), and hydrothermal vents (Connelly et al., 2012; Yoerger et al., 2007). Anthropogenic plumes include pollution from point sources, such as sewage outfalls (Jones

et al., 2015; Rogowski et al., 2012), oil well leaks (Shukla and Karki, 2016), pipeline leaks (McStay et al., 2005), offshore munitions dumps (Adams et al., 2013; Beck et al., 2019), industrial waste disposal at sea (Kivenson et al., 2019) and nutrient enrichment resulting from aquaculture (Jansen et al., 2018). In future, the deep sea mining of metal nodules may also create plumes which will also require monitoring (Spearman et al., 2020).

The mapping techniques used to understand these analogues provide insight relevant to monitoring for potential CCS leaks. The chemical plume caused by the Deepwater Horizon spill in 2010 resulted in many advances in plume mapping with Autonomous Underwater Vehicles (AUVs) (Choyekh et al., 2017; Kato et al., 2017; Shukla and Karki, 2016). Compared to traditional ship-based sampling, AUVs can operate over large areas and can conduct adaptive route planning to track features (Hwang et al., 2019). To transmit data AUVs are required to leave the survey area, sacrificing mission time to travel to and from the surface. This limitation can be addressed by combining AUVs with a surface unit, either a buoy or Autonomous Surface Vehicle (ASV), which can harvest the data from the AUV and transmit it to remote users (Guerrero-González et al., 2016). In comparison, Remotely Operated Vehicles (ROVs) are tethered to ships enabling large amounts of data to be relayed in real time; a benefit when fast leak detection and response is critical. However the disadvantage of this is that a ship is required to operate which adds considerable cost. Monitoring of oil spills and offshore munitions dumps have highlighted the need for appropriate *in situ* sensors to measure different chemical plumes (Adams et al., 2013; Dock et al., 2010; PIECA, IOGP, 2014; Moodie et al., 2010) and this also holds true for offshore CCS.

Gliders are being increasingly used to monitor biogeochemistry in the oceans (Bushinsky et al., 2019; Chai et al., 2020; Vincent et al., 2018), and have even been used to map sewage plumes (Jones et al., 2015). However, the limited ratio of vertical to horizontal distances covered by gliders, combined with their requirement to stay clear of the seafloor makes them unsuitable for mapping fine scale plumes close to the seabed. Previous work concluded that an underwater vehicle would need to operate at an altitude of less than 7 m above the seabed to be able to detect a plume of CO_2 released from the seabed (Dean et al., 2020). ROVs are well suited to mapping plumes as they can achieve this low altitude and the fine positioning control required to operate around subsea infrastructure, such as found around oil and gas rigs and wellheads.

Previous studies have pointed to the benefit of using multiple vehicles to collect data (German et al., 2012; Guerrero-González et al., 2016). This has been suggested for CCS monitoring, using an AUV to monitor a large area and then deploying an ROV to quantify the leak more accurately (Blackford et al., 2014; Dean et al., 2020). ROVs are

routinely used for offshore oil and gas operations (Shukla and Karki, 2016) and can also collect environmental samples. Examples of sampling relevant to CCS monitoring includes sediment cores (Lichtschlag et al., 2015) and water samples, both of which can be processed at a later time in using state of the art analytical instrumentation.

A leak of CO_2 from a marine CCS site would alter the local marine carbonate chemistry. There are four parameters of the oceanic carbonate system which, together with measurements of the water's physical properties (temperature, salinity and pressure) can be used to describe fully the marine carbonate system. These four parameters are the pH, Dissolved Inorganic Carbon (DIC), Total Alkalinity (TA) and fugacity of CO_2, which are described fully in Supplementary Table 1 (Dickson, 1981; Dickson et al., 2007). It is sufficient to measure two of the four parameters and derive the others (Millero, 2007; Williams and Follows, 2011; Wolf-Gladrow et al., 2007). In the case of a CCS leak, the addition of CO_2 to seawater would increase the DIC concentration within the plume and lead to the formation of carbonic acid, which will dissociate to produce bicarbonate and carbonate ions. This will produce protons (H^+), lowering the pH of the water within the plume. Historically studying the marine carbonate system relied exclusively on careful laboratory analysis of collected discrete water samples (Bockmon and Dickson, 2015; Dickson and Goyet, 1994). More recently sensing technology has dramatically improved, and sensors have become increasingly compact and affordable (Wang et al., 2019). A prime example of this is the pH sensor based on Ion Sensitive Field Effect Transistors (Bresnahan et al., 2014; Martz et al., 2010) now commercially available and widely deployed on biogeochemical Argo Floats (Roemmich et al., 2019) and more recently deployed on gliders (Saba et al., 2019; Takeshita et al., 2021).

Models are often used to enhance studies, as collecting data over large spatial scales for extended periods can be both impractical and prohibitively expensive. In the case of CCS monitoring, models have been developed to assist identifying whether a change in water chemistry is due to natural variability or the result of a leak (Blackford et al., 2017). Models have also been used to investigate the dynamics of natural plumes of CO_2, which have been utilised as a proxy for a release from a CCS site (Gros et al., 2019). Models can also be used to guide future experimental sampling. In the context of CCS monitoring, modelling has been undertaken to study optimal survey paths for vehicles to detect plumes (Alendal, 2017).

In this paper we describe how an ROV equipped with a suite of novel sensors was used to monitor a plume resulting from a controlled subseabed CO_2 release as part of the European Union Horizon2020 project titled Strategies for Environmental Monitoring of Marine Carbon Capture and Storage (STEMM-CCS). An overview of the CO_2 release experiment is provided elsewhere in this issue (Flohr et al., 2021). The focus of the STEMM-CCS project was to improve understanding of CCS in the marine environment. Here we compare the results of three different pH sensors with different operating principles (spectrophotometric, fluorescence, and electrochemical) then discuss the benefits and limitations of each sensor. We then develop a parameterised forward model based on the experimental results to expand the sparse spatial coverage of the survey data. We demonstrate how such a model can be used during the planning phase to define the technical specifications of the autonomous vehicles and sensors required to conduct long-term monitoring of an offshore CCS project. This approach could be expanded to inform the design of plume monitoring programmes for other applications.

2. Methods

2.1. STEMM-CCS

2.1.1. Experiment overview

The four-year STEMM-CCS project culminated in a six-week cruise in the North Sea in spring 2019 to carry out a controlled gas release,
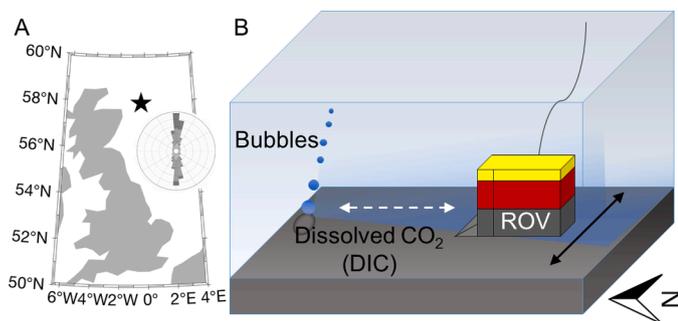
Fig. 1. (A) Map of the United Kingdom, with the experimental site denoted by the star. The overlay shows the current directions at the experimental site, where dark grey sections show currents between 20 and 30 cm s^{-1}, typical currents were 15–25 cm s^{-1}. (B) Schematic illustrating the transects taken by the ROV to conduct the plume mapping. The white dashed arrow illustrate the longitudinal (north-south) transects, along the current direction. The black solid line illustrates the lateral transects, perpendicular to the current direction.

Table 1
Comparison of pH sensors on the ROV.

pH Sensor	Accuracy	Precision	Time per sample	Depth rating	Housing dimensions	Developmental StatusAs Deployed(Current)
LOC pH[1]	< 0.010	<0.001	10 min	6000 m	Ø 12 cm × 20 cm	Prototype (Commercially available)
pH Optode[2]	0.050	0.005	1 s	4000 m	Ø 6 cm × 27 cm	Prototype (Commercially available)
Deep SeaFET[TM][3]	± 0.050*	0.004*	1 s	2000 m	Ø 15 cm × 40 cm	Prototype (Commercially available as part of the Deep SeapHOx[TM])

[1] Rérolle et al. (2012)
[2] Staudinger et al. (2018)
[3] Martz et al. (2010)
* These are values stated by the commercial manufacturer for this model (Sea-Bird Scientific Ltd, USA) users of different models have reported improved values, detailed further in Section 4.1.

analogous to a sub-seabed CO_2 leak in waters ~120 m deep. The experiment consisted of three phases. During phase one the experimental site was prepared. A gas tank was deployed and positioned on the seafloor. The tank (5.5 m long, 2.6 m wide, 2.0 m high and gross weight 13 t) was placed 100 m from the release site. This separation was to prevent the tank influencing the plume dynamics by altering fluid flows around the release site. After the tank was positioned, a curved release pipe was inserted into the sediment at the release site and connected to the tank by a hose. In phase two, the gas flow began generating the plume. During this phase, the gas flow rate was increased incrementally from 6 kg day^{-1} to 143 kg day^{-1}. The third phase dealt with the removal of the tank system and the associated infrastructure, including landers and other observational systems. The experiment involved the coordination of two international research vessels and is fully described elsewhere (Flohr et al., 2021).

2.1.2. Experimental site

The location of the experimental site was in the British sector of the North Sea, approximately 150 km northeast of Aberdeen, Scotland, (Fig. 1A). The site was selected as it is close to a depleted gas reservoir (the Goldeneye gas platform) which was previously identified as a potential CCS reservoir (Spence et al., 2014). The plume was created by releasing gas through a pre-curved pipe inserted with its exit ~3 m deep in the sediment. The gas would pass through the sediment before emerging at the seabed, generating a stream of bubbles in the water column. The sediment in the area was fine sandy clay (Connelly, 2019).

2.1.3. Baseline conditions and natural variability

As part of the experiment the baseline water column conditions at the site were monitored over several years (Esposito et al., 2021) and were also investigated using models (Blackford et al., 2020, 2017). Modelling suggested that seasonal variability in pH within the experimental site was in the order of 0.1 to 0.2 (Blackford et al., 2017). In the summer, stratification of the water column isolates the bottom water from the atmosphere and the remineralisation of sinking biological material lowers the pH of the water close to the seabed. The lowest pH water is typically found in autumn to winter. Winter mixing raises bottom water pH, as deep water mixes with higher pH water from the surface. This is supported by observational data; between October 2017 and April 2018 the bottom water pH had a range of 0.13, with a low of 7.91 recorded in late November to a high of 8.04 in April (Esposito et al., 2021). Models predicted the daily pH variability to be in the order of 0.001 (Blackford et al., 2017). The region experiences a 1.7 m tidal range, and this drives the prevailing currents, orientated to the north-south. Data collected during the cruise demonstrated that the maximum current magnitude within 1.2 m of the seafloor was between 10 and 30 cm s^{-1}, and for 80 % of the experimental period the predominant current directions were orientated within 30° of north or south (Fig. 1A, overlay). During the experiment in May 2019, Esposito et al. (2021) found that close to the seafloor the tidal variability in pH was in the order of 0.008.

2.2. ROV survey description

For the STEMM-CCS experiment the ROV Isis was utilised to position various sensor platforms around the gas release site. The ROV Isis is rated for depths of 6500 m and can be classified as a work class ROV. Equipped with two manipulator arms, it is capable of high-precision spatial control. This fine control was essential for deploying multiple seabed landers around the gas release site, without overly disturbing the sediment. Equipped with various sensors, these landers collected data described elsewhere in this issue (Flohr et al., 2021; Schaap et al., 2021). During the longer overnight dives the ROV was manoeuvred to map the spatial extent of the plume. Longitudinal (north-south) surveys aligned with the prevailing currents were conducted, as illustrated in Fig. 1B. For these longitudinal surveys the ROV transect started at the point of bubble emission and finished 10 m downstream. These surveys were conducted at two altitudes; 1.5 m and 3.5 m above the seafloor. During these surveys the ROV paused at each 1 m interval downstream, holding its position for a minimum of 10 min to collect replicate measurements. A lateral transect was carried out to determine the extent of the plume perpendicular to the prevailing current. The lateral transect was taken 6 m downstream of the bubble stream, at an altitude of 1.2 m. During the lateral transect the ROV paused approximately at each 0.5 m interval holding position for a minimum of 10 min. Lastly the ROV performed vertical profiles where it maintained position at different altitudes above the plume. When transiting between measurement stations the ROV travelled at a speed of ~10 cm s^{-1}; this low speed meant the ROV did not appear to sway considerably once it stopped at each measurement point.

2.3. Sensors

To measure the changes in pH caused by the released CO_2, three different *in situ* pH sensors were mounted on the ROV. The sensors used in this experiment are summarised in Table 1 and further details on each are provided inthe following sections. The physical location of each sensor was recorded relative to the ROV's central reference point and this information was used during the data processing to correct for the shifting currents. As the surveys were carried out at various stages in the tidal cycle, the downstream position of the plume shifted relative to source and hence ROV position. This was corrected for during post processing to give each data point a longitudinal distance from the bubble streams and lateral distance from the plume's central axis of travel, adjusted for the current direction and the sensors physical location on the ROV. Alongside the pH sensors, the ROV was also equipped with six 1.7 l Niskin bottles and a FastCAT 49 CTD (Sea-Bird Scientific, USA) which provided the temperature, salinity and depth data used in the processing of the pH measurements.

2.3.1. LOC pH sensor

A miniaturised spectrophotometric "lab-on-chip" (LOC) sensor was used to make accurate pH measurements during the ROV surveys (Rérolle et al., 2012; Yin et al., 2021). The pH sensor is based on a LOC platform technology proven through its use in nutrient monitoring on stationary and moving platforms (Beaton et al., 2012; Clinton-Bailey et al., 2017; Grand et al., 2017; Vincent et al., 2018). The pH LOC sensor
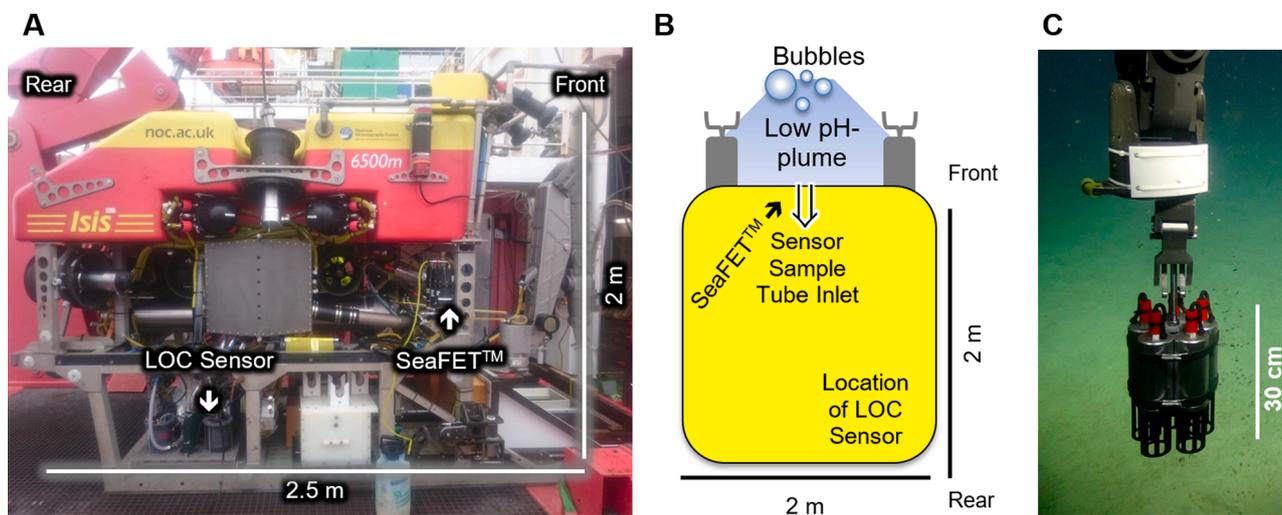
Fig. 2. Location of the sensors on the ROV. (A) Side view of the ROV, showing the location of the LOC and SeaFET™ sensor. (B) Plan view of the ROV. (C) The optode bundle held by the ROV manipulator.

is based on the standard spectrophotometric pH technique utilising purified m-Cresol Purple (Clayton and Byrne, 1993). This method can achieve a pH precision better than 0.001 and accuracy better than 0.010 with little to no long-term drift (Yin et al., 2021). Each measurement is blank-corrected and pH is calculated by the ratio of absorbances at two wavelengths and is therefore immune to long-term drift caused either by changes in light source intensity or detector sensitivity. A limitation of the LOC pH sensor for this application is its measurement frequency; each measurement takes 10 min, which is slow for use on a moving platform in a dynamic region. This 10 min measurement comprises a flushing cycle, a 30 s sample collection phase, and finally a measurement phase during which the collected sample is analysed. To complement this data other sensors were selected with faster sampling frequencies.

The LOC sensor was mounted in the rear right quadrant of the vehicle, as shown in Fig. 2 Panels A and B. To ensure that the LOC sensor was measuring as close to the plume as possible, a submersible pump (SBE-5M, Sea-Bird Scientific, USA) continuously flushed seawater through a flexible tube (2.8 m long, ~15 mm inner diameter) from the front of the ROV back towards the sensor. The inlet of this pump was located 20 cm above and 32 cm behind the central reference point of the ROV. The intake port of the sensor was inserted into this tube near its outflow point at the back of the ROV. The sensor was fully integrated into the ROV, receiving power from the vehicle and transmitting data in real time back to the control room on the surface. The LOC sensor deployed in this experiment was produced at the National Oceanography Centre, Southampton. These sensors are now manufactured and sold under license (ClearWater Sensors Ltd., UK).

2.3.2. Optodes

The plume was also monitored using newly developed pH and oxygen optodes. The optode systems are good candidates for use in autonomous system as they are lightweight, small, do not use reagents and have low power consumption. The pH and oxygen optode sensors used in this experiment were developed at the Technical University Graz and PyroScience GmbH (Aachen, Germany). The sensors deployed in this experiment were prototypes, however these devices are now commercially available (PyroScience GmbH, Germany). The optodes consist of two essential components: pH (or O_2) sensing material and the read-out module. The pH sensing material utilises the pH-dependent fluorescence of an aza-BODIPY indicator dye (Staudinger et al., 2019). The dye is immobilized into a proton-permeable polymeric matrix (hydrogel). A reference material with a pH-independent long-lived emission is added to this layer to enable phase shift read-out according to the Dual Lifetime Referencing Technique (Klimant et al., 2001). The spots of the sensing

material are glued to a screw-on cap adaptor that is connected to the logger unit. The prototype of the opto-electronic unit was described elsewhere (Staudinger et al., 2018). The logger unit used in this work underwent major modifications with respect to optical feed-through, temperature sensor, and the pressure housing which was changed from polyoxymethylene (POM) to titanium. The logger in the titanium housing has small dimensions (63 mm diameter, 270 mm length) and weight in water of 0.85 kg. The power consumption is low (~1 mW at an acquisition rate of one measurement point in 10 s) which makes it suitable for autonomous operation during several months, as demonstrated during a two-month deployment (Fritzsche et al., 2018).

Three individual pH optodes and two oxygen optodes were mounted together to form a single unit, shown in the ROV manipulator in Fig. 2 C. The oxygen optodes were included for referencing purposes, as no change in oxygen concentration was expected in the plume. The optodes were held by the ROV's manipulator arm throughout the surveys, and on three occasions were held directly into the bubble stream to measure the direct effect of the CO_2 plume. When not actively surveying the optodes were stowed in a basket on the ROV's front deck.

2.3.3. SeaFET™

An early version of the Deep SeaFET™ (Sea-Bird Scientific Ltd., USA) was mounted on the ROV for the plume surveying work. The SeaFET™ uses an ion sensitive field effect transistor (ISFET) to measure pH changes. The pH of the fluid contacting the ISFET controls the surface charge at the interface which determines the electric field in the transistor (Martz et al., 2010). The SeaFET™ was selected as it had a rapid sampling frequency of 1 Hz and this version was depth rated to 2000 m (Johnson et al., 2016). Although it can measure more rapidly than the LOC pH sensor it has a lower pH accuracy stated as ± 0.050 on the manufacturer's specifications. The version of the Deep SeaFET™ used in this experiment is not currently commercially available as a standalone sensor, but is available integrated with other sensors as part of the Deep SeapHOx™. A compact version is being used on profiling floats and, more recently, was modified to be integrated on ocean gliders (Saba et al., 2019; Takeshita et al., 2021).

The SeaFET™ sensor needs to be conditioned in the target seawater (Bresnahan et al., 2014) so for this deployment the sensor was soaked in seawater from the experimental site for a period of ten days prior to commencing the surveys. To protect the ISFET from potential knocks an open guard was used. This was selected as in this deployment the SeaFET™ was not connected to a pumped CTD and the open guard allowed more efficient flushing of the sensor head than the standard flow cell. The pH was calculated using the equations previously reported

(Johnson et al., 2016) and temperature, salinity and depth data was collected by the ROV.

The SeaFET™ was mounted on the front of the ROV. To ensure that the sensors sampled the same water it was mounted close to the inlet of the tube providing samples to the LOC sensor (Fig. 2 A and B). The sensor was internally powered and logged data internally as a stand-alone sensor.

2.4. Model

A model of the propagation of the DIC-enriched plume water from the CO_2 release was created using COMSOL Multiphysics® modelling software. This model was designed to replicate only the highest CO_2 release rate and only during a quasi-steady-state southbound current. The majority of the survey data were collected during this release rate which was the closest to (although still far below) the maximum leakage rate relevant to an offshore carbon storage facility at the location where the experiment took place (Flohr et al., 2021). This model was fitted to the sparse spatial data collected during the surveys. As the release rate of the gas was known, the model was used to estimate the fraction of CO_2 retained within the sediments.

The model operates on a 200 m × 6 m × 6 m cuboid. The current moves in the x direction (the length of the cuboid). The z direction is the altitude above the seafloor, and y is the transverse direction parallel to the seafloor. The advection of the plume is modelled with the Transport of Diluted Species module.

The current U is defined as

$$U(z) = \frac{U_{shear}}{\kappa} \log\left(\frac{z}{z_o}\right)$$

where U_{shear} is 0.0073 m s^{-1}, $\kappa = 0.41$ (von Karman's constant), and $z_o = 2 \times 10^{-4}$. U_{shear} and z_o are determined by both the local hydrodynamics and sediment surface conditions, these values were estimated from measurements taken at the site (Schaap et al., 2021).

The turbulent diffusion coefficient of the DIC is

$$D_t = U_{shear}\kappa z$$

The background DIC concentration (C_0) was set at 2133 mol m^{-3}, based on the DIC concentration of the seawater derived from the CO2SYS software package (Lewis and Wallace, 1998; van Heuven et al., 2011) using the average background values measured at the experimental site. The average (±standard deviation, n) background values are: pH = 8.046 (± 0.001, $n = 5$), TA = 2302 μmol kg^{-1} (± 14 μmol kg^{-1}, $n = 13$) phosphate = 0.61 μM (± 0.08 μM $n = 282$), silicate = 3 μM, pressure = 119.5 dbar (± 0.5, $n = 282$), temperature = 7.74 °C (± 0.04 °C, $n = 282$), and salinity = 35.25 (± 0.02, $n = 282$). The carbonic acid dissociation constants used were those from (Mehrbach et al., 1973) refit by (Dickson and Millero, 1987) coupled with the KSO_4 dissociation constant in (Dickson, 1990) and the oceanic concentration of total boron from (Uppström, 1974). Temperature and salinity values came from a SeapHOx™ sensor (Sea-Bird Scientific, USA) mounted on a lander located 375 m to the southeast of the release site. The phosphate concentrations were taken from a lab-on-chip phosphate sensor (Clinton-Bailey et al., 2017; Grand et al., 2017) on the same lander. Each of these parameters was measured every 2 h for 23 days resulting in 282 measurements. The silicate value was an estimate based on the silicate-phosphate ratio measured in the region during previous expeditions (Esposito et al., 2019). The total alkalinity was measured by a lab-on-chip total alkalinity sensor (Wang et al., 2019) located on the ROV during the same survey dive. The pH values described above were made by the LOC pH sensor (detailed in Section 2.3.1), and were taken over the course of an hour while the ROV was conducting off-site operations following a survey transect.

At the $x = 0$ plane, the concentration of DIC from the release (C_z) is based on a model of the dissolution of CO_2 bubbles (Dewar et al., 2015)

Table 2
Details of each dive, highlighting the sensor configurations and the gas release rate.

Dive Number	Dive Description	Gas Release Rate kg day^{-1}	LOC	Optode	SeaFET™
360	Longitudinal Transect And Vertical Profile	5.7	✓	✓	
366	Longitudinal Transect And Vertical Profile	28.6	✓	✓	
372	Longitudinal Transect And Vertical Profile	85.8	✓	✓	✓
376	Lateral Transect	143.0	✓		✓

using a 4 mm diameter bubble size, which was based on experimental observations:

$$C_z = C_O + a_1\left(1.5 - z^{0.65}\right) * |a_2 - y|$$

with $a_1 = 0.04$ provided the best fit to the experimental data, and $a_2 = 1.8$ chosen to represent the ~3.6 m spread of bubble vents, observed with the ROV, on the seafloor during the experiment.

As outputs, the model can be used to estimate the total mass flow rate of DIC coming from the CO_2 release by integrating the x-direction DIC flux on one entire y-z plane. The difference in this flux with and without the modelled CO_2 source yields the excess DIC flux from the release.

An important use of the model is to inform the design and specifications of future subsea CCS monitoring approaches. We demonstrate this approach by defining a detectability threshold based on a pH change of 0.010 under the environmental conditions of the release experiment. This threshold was selected as it is at least double the precision of each of the *in situ* pH sensors used in this experiment. Furthermore, it allows for direct comparison with models done before the experiment (Blackford et al., 2020). This pH decrease is equivalent to an increase in DIC of 4.3 μmol kg^{-1} as determined by the CO2SYS MATLAB® script using the conditions described above (Lewis and Wallace, 1998; van Heuven et al., 2011).

3. Results

3.1. pH sensor data

The ROV was in operation nearly continuously throughout the gas release experiment, as it deployed various seabed instrumentation and operated the gas flow controls of the gas rig (Flohr et al., 2021). Overnight, the ROV was occasionally used to conduct plume surveys using the on-board pH sensors. Presented here are the pH measurements taken during four such overnight dives. The surveys were conducted during four different CO_2 flow rates, with the full details of each dive presented in Table 2. The SeaFET™ was also used on other vehicles during the release experiment and therefore was not present on the ROV for dives 360 and 366. Similarly, the optodes were not used on dive 376 as this dive happened at short notice. The pH scale used throughout this paper is the total proton scale (as described in Supplementary Table 1).

The data from each pH sensor are presented as the difference relative to baseline pH. This difference is referred to as the pH anomaly. The baseline pH was measured for an hour during each dive, when the ROV was at least 100 m away from the CO_2 bubble stream. The optodes and SeaFET™ recorded data at 1 Hz, a higher frequency than the LOC sensors. To enable comparison these data were averaged over a 30 s period commencing when the LOC sensor started to sample. All sensors measured baseline pH within the precisions values stated in Table 1, and the standard deviations of the measurements taken by each sensor during the baseline calculation are presented in Supplementary Table 2.
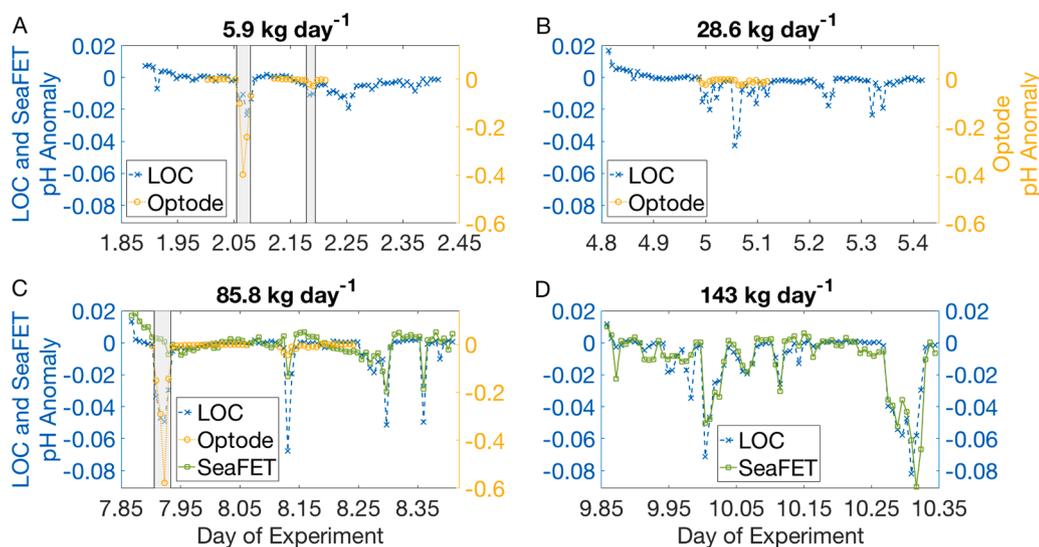
Fig. 3. Plot showing the pH anomaly (relative to the pH at a point outside the influence of the gas release) recorded when the ROV surveyed the plume, with a separate panel for each of the four dives (A,B,C and D). The day of the experiment is decimal days after the gas flow was started. The grey boxes highlight when the optodes were deployed directly into the bubble stream. Note in panels A, B and C the optodes scale is on the right of each plot while the LOC and SeaFET™ share the left hand axis in all panels.
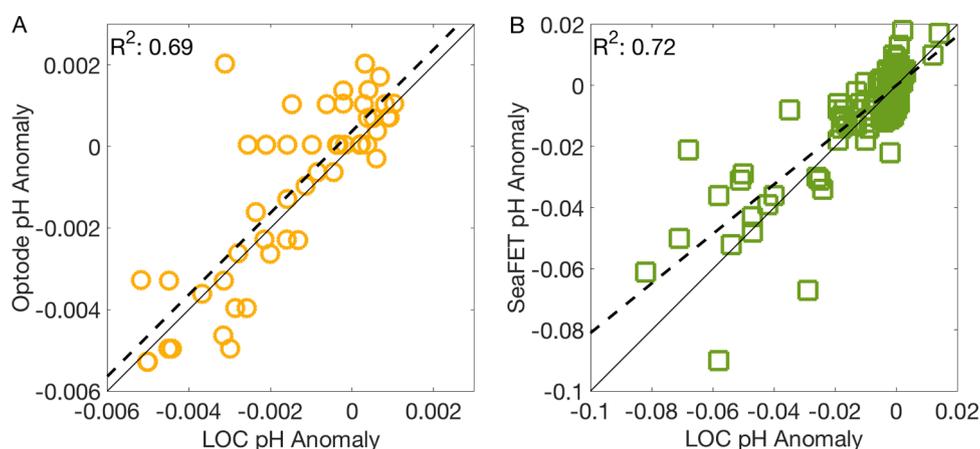
Fig. 4. (A) Relationship between the pH anomaly as recorded by the LOC and the optodes, excluding the times when the optodes were directly in the bubble stream. (B) The relationship between the pH anomaly as recorded by the LOC and the SeaFET™ sensors, excluding a subset of data from dive 372. In both panels the dashed line shows the regression lines and the solid line the 1:1 line.

The average standard deviation of the baseline measurement across all dives recorded by the three optodes was 0.001. This was well below their reported precision of 0.005, and for this reason, the data from the three optodes were pooled together.

In each panel of Fig. 3 the negative pH anomaly shows the presence of additional CO_2 in the water column, after the commencement of the gas release on the 11th May 2019. The grey boxes in Fig. 3 indicate when the optodes were inserted directly into the bubble stream. When inserted into the centre of the bubble stream the optodes recorded a pH anomaly of -0.400 and -0.580 at the gas release rates of 5.9 kg day^{-1} and 85.8 kg day^{-1}, respectively (Fig. 3, A and C). These drops are 17 and 8 times larger, respectively, than those simultaneously recorded by the LOC outside of the bubble stream. When the optodes were outside the bubble stream the measured drop in pH was similar to those observed by the LOC sensor. Excluding all the optode data recorded directly in the bubble stream, the relationship between the pH anomalies recorded by the optodes and those recorded by the LOC sensor can be described $pH_{anom\_optode} = 1.003 \times pH_{anom\_LOC} + 0.0004$ ($R^2 = 0.69$, $p < 0.005$, $n = 50$, $SE_{regression} = 0.001$), shown in Fig. 4A. As expected, the oxygen data recorded by the optodes detected no impact of the CO_2 release, as no oxygen was released during the experiment.

Throughout the dives with the highest gas release rates there was good agreement between the SeaFET™ and the LOC sensor. When the

CO_2 release rate was 85.8 kg day^{-1} there were two periods when the agreement between these two sensors was not good (Fig. 3C). Around day 7.9 the LOC sensor captured evidence of the plume which was not seen in the SeaFET™ data. At this time the LOC sensor recorded an anomaly of ~-0.04 yet the SeaFET™ did not record a noticeable pH anomaly. During that time the currents were relatively strong, with a flow of ~0.2 m s^{-1} originating directly behind the ROV, so it is possible that the SeaFET™ sensing element was not being effectively flushed. At day 8.14 the LOC sensor recorded an anomaly of ~-0.06 while the SeaFET™ recorded a smaller anomaly of ~-0.02. This occurred shortly after slack tide and around this time the ROV had been operating close to the seabed recovering an instrument. Excluding these data, there was generally a good agreement between the pH anomaly measured by the SeaFET™ and the LOC sensor described by: $pH_{anom\_SeaFET} = 0.811 \times pH_{anom\_LOC} + 0.00002$ ($R^2 = 0.72$, $p < 0.005$, $n = 146$, $SE_{regression} = 0.008$, Fig. 4B). Both the LOC and SeaFET™ sensors recorded data most of the time the ROV was in the water. On several occasions the LOC and SeaFET™ detected the CO_2 plume while the ROV was operating within the CO_2 release site but not actively mapping the plume. When the CO_2 release rate was 85.8 kg day^{-1} the largest pH anomalies recorded by both the LOC and SeaFET™ sensors were made at day 8.3, while the ROV was collecting gas samples from the centre of the bubble stream (Fig. 3C). The largest magnitude anomaly of ~-0.08 recorded by both
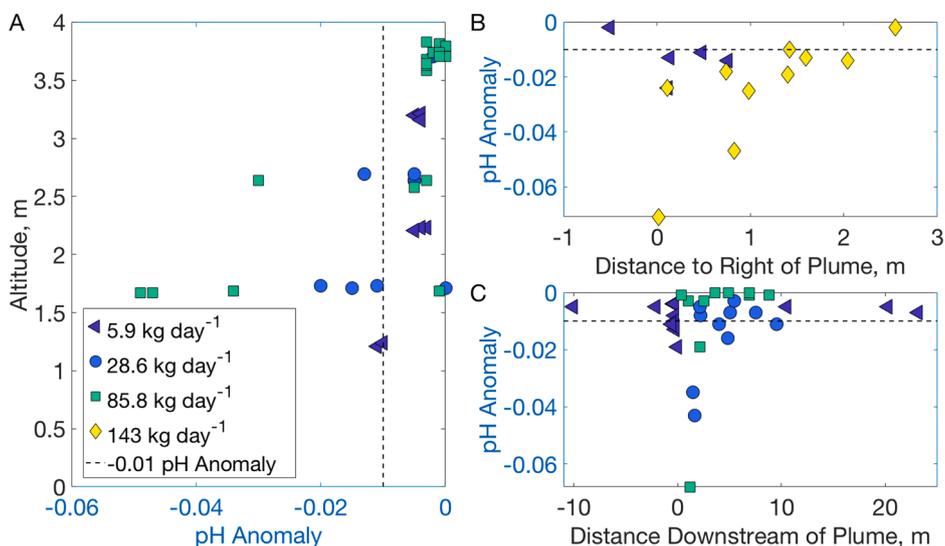
Fig. 5. (A) Vertical profiles from dives 360, 366 and 372. (B) Lateral transects. (C) Longitudinal transects. In all panels a dashed line indicates the pH detectability threshold (0.010 units) and the symbols the gas release rate, following the legend in panel A.
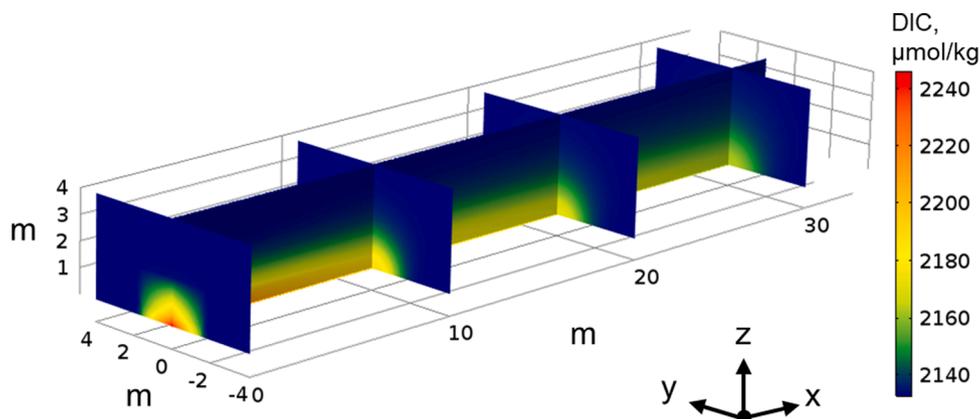
Fig. 6. Snapshot of the plume model. The source at $x = 0$ m represents the CO_2 release; the plume dynamics are driven by the current in the x direction along with turbulent diffusion in the y and z directions.
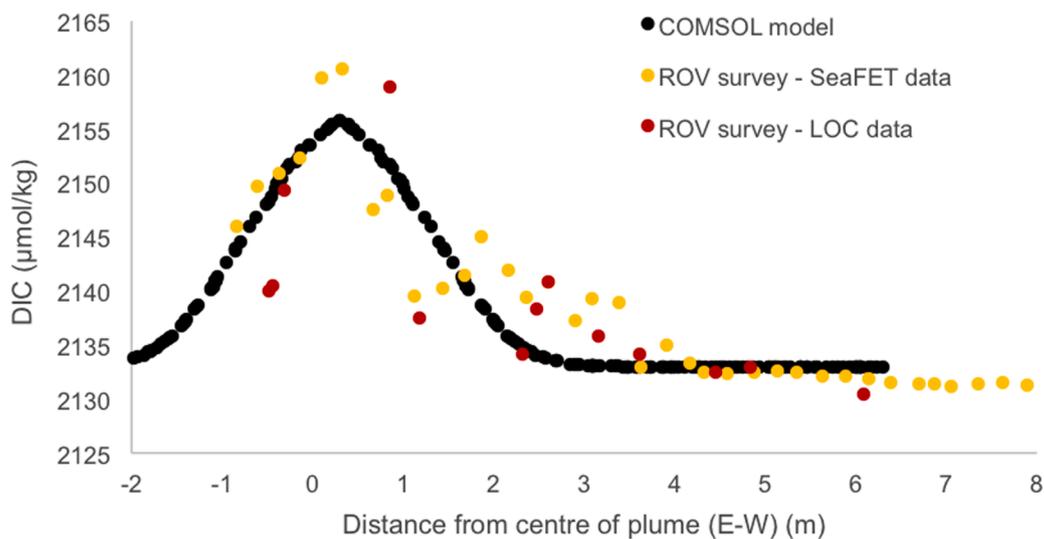
Fig. 7. Model outputs compared to two pH sensors for the lateral transect survey.
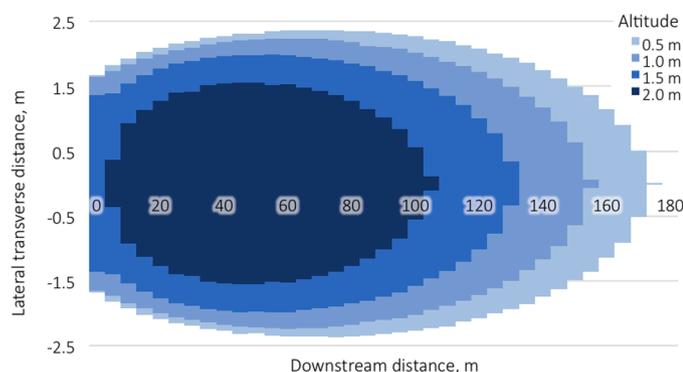
Fig. 8. Top-down view of regions with a detectable pH change (pH decrease of magnitude > 0.010) under the CO_2 mass flow rates and hydrodynamic conditions of the CO_2 release experiment, at planes of constant altitude above the seafloor.

the LOC and SeaFET™ sensors was on day 10.3 (Fig. 3D). At this time the release rate was 143 kg day^{-1} and the measurements were made while the ROV was collecting sediment push cores from the centre of the gas release site.

It was anticipated that the largest impact of the released CO_2 on water chemistry would be adjacent to the seafloor, due to the rapid dissolution of gaseous CO_2 in seawater. To determine the vertical extent of the plume, pH profiles were measured vertically during dives 360, 366 and 372. The data from the LOC sensor profiles are shown in Fig. 5A. In all profiles the largest pH anomalies were measured closest to the seabed. When the gas release rate was 5.7 kg day^{-1} there was no detectable plume signal, as indicated by the lack anomalies below -0.01 (dark triangles in Fig. 5). When the gas release rate was increased to 28.6 kg day^{-1} negative pH anomalies less than -0.01 were recorded below 2 m (circles in Fig. 5). When the release rate was 85.8 kg day^{-1} pH anomalies of up to -0.049 were recorded (squares in Fig. 5). The plume remained undetectable higher than 3 m from the seabed throughout the profiles. The lateral transect data are shown in Fig. 5B, and at a release rate of 143.0 kg day^{-1} the pH anomaly was detectable within ~ 1.5 m to the right of the plume centre (diamonds in Fig. 5B). The longitudinal transects in Fig. 5C show that plume was detected downstream of the plume centre, most notably within ~ 5 m of the plume centre.

3.2. Plume model

The COMSOL model of the plume is shown in Fig. 6. The bubbles enter the water column at the plane defined by $x = 0$ m. The spatial distribution of the plume is heavily dominated by the low-altitude source of the DIC and the currents.

The output of the model at 6 m downstream of the release site ($x = 6$ m, $z = 1.2$ m above the seafloor) can be directly compared to the ROV's east-west lateral transect survey (1.2 m $> z < 1.5$ m) (Fig. 7).

3.3. Plume detectability

Prior to the CO_2 release experiment, models were developed to predict the extent of the plume (Blackford et al., 2020). These models provide an estimate of the spatial extent of the CO_2 plume as a function of the CO_2 release rate. The spatial extent of the plume was defined by a pH perturbation threshold easily detectable above natural variability using state of the art pH sensors. Two thresholds were studied: pH change > 0.010 and pH change > 0.100 pH units. The 0.010 pH threshold is considered more relevant for detectability as it is beyond the likely high frequency natural variability of the system, while the 0.100 threshold is considered more relevant for ecological effects. Based on the smaller threshold, pre experiment models predicted a CO_2 plume volume of 815 m^3 from a release rate of 143 kg day^{-1}. The volume of the

CO_2 plume derived by the COMSOL model and sensor observations was 1024 m^3, using a DIC threshold of > 4.3 μmol kg^{-1} (i.e. a pH change of > 0.010 under the conditions at the CO_2 release experiment site). Using the larger pH threshold (i.e. a pH change of > 0.100) the pre-experiment model predicted a CO_2 plume volume of 21 m^3 while the data-based COMSOL model predicted a plume volume of 17 m^3.

Fig. 8 shows the spatial distribution of the CO_2 plume from the COMSOL model on planes parallel to the seafloor. The shape of the plume was characterised by being low to the seafloor (< 2 m altitude), long, and narrow. At 2 m altitude, the plume was only 3 m wide in the transverse direction, but 100 m long along the main direction of the current. Closer to the seafloor, at 0.5 m altitude, the plume was larger: a maximum of 5 m wide and 170 m long.

4. Discussion

4.1. pH sensor data and comparison

Over the course of the plume mapping surveys all three different sensors generally recorded pH changes of similar magnitudes. At the highest CO_2 release rate of 143 kg day^{-1} the LOC recorded a pH anomaly of -0.081 and the SeaFET™ -0.090, when the vehicle was within 2 m of the seabed. This demonstrates that both sensors recorded the same parcel of water and both could detect the plume. The optodes recorded the largest pH anomaly of -0.580 when positioned directly into the bubble stream when the CO_2 release rate was 86 kg day^{-1}. This decrease was an order of magnitude greater than any measured by the other sensors because this measurement was made directly in the centre of the plume where the effect of the leak was the greatest. There were occasions when the LOC and SeaFET™ recorded different pH anomalies. Notably during day 7.9 the SeaFET™ did not measure the plume, this is potentially the result of the sensing element not being flushed fully due to the way the sensor was mounted on the ROV frame. This highlights a key requirement in future deployments to ensure any sensors are mounted to maximise their flushing, or ensure a pumped system is used.

Each type of pH sensor has different strengths and weaknesses. The LOC sensor offers higher accuracy and precision than the other technologies. However each measurement requires more time to process (~ 10 min), because it involves water sampling, reagent mixing followed by optical measurements (Yin et al., 2021). Although relatively slow, the accurate and high precision measurements of the LOC means it is more likely to detect smaller CO_2 leaks. On fast-moving platforms the spatial resolution of LOC pH measurements will be limited by its measurement frequency, with the potential risk of missing spatially isolated leaks. On stationary platforms, such as seabed landers, the LOC pH sensor offers long term, high performance measurements. This makes it suitable for detecting subtle long-term changes in pH that may be associated with non-point source CO_2 leaks gradually increasing over time. Furthermore, if positioned at high-risk locations, such as wellheads, the LOC pH sensor offers the highest sensitivity for long term monitoring. The high accuracy measurements of the LOC sensor also make it a good choice for conducting follow up surveys of any potential leaks initially detected using an AUV equipped with a faster but less accurate pH sensor. Under this scenario it could be envisaged that an AUV equipped with a higher frequency pH sensor could identify a possible leak signal and trigger a follow up investigation with an ROV for a detailed investigation, and more accurate quantification of the leak. Alternatively, the LOC sensor could be used for periodic calibration of faster but less accurate sensors integrated on AUVs for wide area surveys of CCS reservoirs. Although not as small as other autonomous sensors, LOC sensors have been integrated on gliders (Vincent et al., 2018) and larger AUVs such as the Autosub Long Range (Yin et al., 2021). As each measurement only consumes 3 μL of reagent, the reagent volume carried on board is in the order of 10s of mL with minimum impacts on space availability. One of the main advantages of the LOC pH sensor is its superior depth rating capable of 6000 m (Yin et al., 2021). In comparison, the optodes are

rated to 4000 m, and currently the SeaFET™ is only depth rated to 2000 m. In Europe most of potential offshore CCS sites are located in the North Sea (IEA Greenhouse Gas R&D Programme, D.R.D. 2008) where depths are limited to a few hundred meters. Elsewhere, however, such as off the coast of Brazil, potential CCS sites have been identified at depths greater than 2200 m (Ketzer et al., 2015) which could present challenges for monitoring. In deeper waters, the higher pressure will enhance CO_2 dissolution and reduce the size of bubbles, making visual or acoustic identification of a leak challenging. In this scenario chemical-based leak detection may be the only option, using chemical sensors with the required depth rating.

The optodes are small, self-contained and completely autonomous sensors capable of high frequency measurements. These attributes make them ideal candidates for mounting on fast-moving autonomous vehicles, capable of surveying large areas more effectively, and at a greater spatial resolution. Their small size and low power requirement would enable integration on the smallest AUVs for long deployments. In this experiment the optodes' small size enabled them to be easily manipulated by the ROV's arm directly into the bubble stream where they recorded the largest pH drop. As demonstrated in this experiment the optodes are small enough that multiple units can be deployed in a small space, which could be an advantage in long deployments, providing redundancy in case of sensor failure. A consideration to be aware of with the optode systems is their temperature dependence (which is compensated by an integrated resistance thermometer) and potential salinity cross-talk. There is no effect of typical oceanic salinity ranges (~15–35 PSU) on the measurement; however, at the lower salinities typical to estuaries (~5 PSU) there can be a measureable effect. However this can be corrected during post processing, provided salinity is recorded (Staudinger et al., 2019). Another potential limitation is a temperature dependant drift caused by degeneration of the indicator dye. This drift can occur over many months in warm waters and is slower in cool water; this could be accounted for if temperature is logged. In future versions of the optodes there is potential that improved materials could eliminate this issue. Co-deploying the optodes with a LOC sensor could mitigate the main limitations of both sensors, as the LOC data could be used to correct the optode drift. Together this sensor pairing could achieve fast and accurate measurements in waters up to 4000 m.

The SeaFET™ is also capable of high frequency data collection allowing good spatial resolution if using a moving vehicle to survey an area. The version of the Deep SeaFET™ used in this experiment had a larger housing to accommodate internal batteries, which limits the size of the vehicle this unit could be mounted on, however there is now a commercially available version integrated on a profiling float (Sea-Bird Scientific Ltd, USA) and this model has recently been modified for various glider deployments (Saba et al., 2019; Takeshita et al., 2021). These recent glider deployments report improved accuracy and precisions compared to the model used in this experiment, which is more similar to that tested by the Alliance for Coastal Technologies (ACT). ACT conducted seawater trials comparing the pH recorded by the Sea-FET™ to reference data (Tamburri et al., 2015). Over three separate deployments in seawater the average and standard deviation of the measurement difference between the SeaFET™ and reference pH was found to be: –0.008 ± 0.029, $n = 84$; –0.014 ± 0.009, $n = 101$; –0.001 ± 0.007, $n = 107$ (Tamburri et al., 2015). The recent glider deployments highlighted other considerations to be aware of when deploying the ISFET style sensors. Saba et al. (2019) found that biofouling was a problem during shallow (< 200 m depth) deployments, demonstrating the need for antifouling measures for deployments in shallow and highly productive waters. Takeshita et al. (2021) confirmed previous findings that ISFET sensors are influenced by exposure to sunlight (Bresnahan et al., 2014; Hemming et al., 2017), which is an important consideration in monitoring pH in shallow regions. Ensuring that the sensor is housed in the dark can mitigate the influence of light on the measurements. Takeshita et al. (2021) also reported a pressure hysteresis that developed over the course of the deployment; this could be an issue if the sensor is

mounted on an AUV which is surfacing repeatedly. A further limitation of the SeaFET™ sensor is that user experience has been found to play a considerable role in determining the quality of data recorded (McLaughlin et al., 2017). In the case of future CCS it is likely that non-expert users will conduct widespread monitoring, and as such key sensor requirements would be ease of operation. This means that if SeaFET™ based sensors were to be widely deployed to monitor CCS the end users would require training to ensure best practises are followed and the data processed correctly. To collect the most accurate data the SeaFET™ sensors require careful calibration or close comparison to bottle samples. Addressing this limitation, a self-calibrating ISFET sensor has been trialled (Bresnahan et al., 2021). This self-calibrating unit requires 4.5 L of reagent as each standardisation uses 150 mL of reagent, resulting in a total package greater than four times the size of the LOC. As the LOC pH sensor only requires 3 μL of reagent per measurement combining a LOC pH sensor with a SeaFET™ could be the optimal way to collect data that is both high frequency and high accuracy.

4.2. Plume model

The plume model shown in Fig. 6 was used to estimate the mass flow rate of CO_2 entering the water column. This estimate was obtained by integrating the total flux of DIC over a y-z plane at $x = 6$ m. The difference between the flux with the CO_2 source turned on and turned off provided a total release rate into the water column of 82 kg day^{-1}. The CO_2 was released into the sediments at a rate of 143 kg day^{-1}, suggesting that slightly over half of the CO_2 escaped from the sediments into the water column. This value is specific to the site and release properties used in this experiment. The migration and behaviour of CO_2 through sediments is a function of many site-specific properties such as stratigraphy, gas volume, and leak rate (Cevatoglu et al., 2015). However, this value is of use for comparing the outcome of this model to other quantification methods, with an overview presented elsewhere in this issue (Flohr et al., 2021), and also for providing contextual data for interpreting other analyses done during the experiment.

Any model has inherent uncertainties, and in particular this model has been parameterised to match experimental data which itself has errors and uncertainties due to instrument and environmental variability. Some instrument bias was mitigated through the use of multiple instruments, but data on the current direction and ROV position have only a single source. The calculation of DIC from pH and TA also contains inherent uncertainties, and the model itself relies on approximation of the bubble emission properties. Despite these uncertainties, we can use the model to inform some qualitative and quantitative observations about how the plume properties drive the technology requirements for CCS monitoring and to establish the importance of hydrodynamic measurements and vehicle selection. A more thorough model study could estimate the uncertainty caused by the model itself through using a range of different model systems, an approach used by Blackford et al. in their model study of CCS seep detectability (Blackford et al., 2020).

4.3. Plume detectability

The plume model showed that the local currents heavily influenced the plume structure and orientation. This model data could be used to plan the trajectories and requirements of an AUV- or ROV-based monitoring system for CO_2 leaks in a CCS context. For example, a vehicle carrying a pH sensor with a precision of 0.010 and a 1 Hz measurement frequency traveling at an altitude of 1.5 m above the seafloor would be able to detect the plume under hydrodynamic conditions of the CO_2 release experiment. A survey conducted at a velocity of 1 m s^{-1}, along tracks spaced 20 m apart and orientated perpendicular to the currents, would yield three pH data points above the detectability threshold on at least five transit lines. In a future plume detection scenario this detected

Table 3
Summary of the benefits and limitations of the sensors deployed in this experiment.

	Benefits	Limitations
LOC	High accuracy, low drift, depth rated to 6000 m	Slow sample frequency
Optode	Rapid sample frequency, small form factor, depth rated to 4000 m	Potential drift in measurement
Deep SeaFET™	Rapid sample frequency, available commercially to mount on float	Requires conditioning, depth rated to 2000 m, experienced user required to collect high quality data

anomaly could then be surveyed in a more targeted monitoring phase, by deploying landers or an ROV with enhanced sensing capabilities to fully quantify the leak.

The modelling has highlighted the importance of the local current magnitude and orientation on plume detection. This is important to consider in other situations when surveying alternate types of plume. If an AUV is used to conduct a lawn mower style survey, ensuring that the tracks are orientated to be perpendicular to the prevailing current will enhance the likelihood of the plume being detected, especially in regions with fast currents, provided that the sensor sampling frequency is matched to the vehicle's velocity. Once an initial plume signal is detected, a follow-up study could be initiated, deploying sensors in a more targeted manner.

In this experiment the low leak rates combined with strong currents resulted in a plume constrained close to the seabed. The experimental site was also densely packed with a number of landers, which meant that an AUV could not be safely operated at a low enough altitude to map the plume. Under these conditions the ROV provided the only means for mapping the plume during this experiment. Under real-life CCS reservoir monitoring scenarios however, AUVs would be better placed for covering larger areas without the need for a ship. In large scale monitoring the cost of operating an ROV over large areas is likely to be prohibitive, so sensors that can be easily integrated into AUVs are desirable. In areas with no seabed infrastructure, or extremely well surveyed areas, piloting an AUV close to the seabed would be possible and potentially the most appropriate sensor platform. AUVs well suited to missions such as this include Autosub Long Range AUV (Furlong et al., 2012), REMUS AUV or SeaBED AUV, which was specifically developed to be manoeuvred close to the seabed and is also capable of hovering over a point (Singh et al., 2002). In regions with lower currents the detectable plume would be expected to reach higher altitudes above the seafloor into the water column. This would allow for detection further above the sea floor, resulting in a lower risk deployment for an AUV, or potentially even the use of gliders. In a scenario when the plume being mapped is likely to be buoyant and conservative, such as an oil spill or hydrothermal vent plume, the requirement to make measurements close to the seabed would be removed, and again AUVs or gliders may prove to be the optimal vehicle for surveying.

5. Conclusions

All pH sensors integrated on the ROV during the STEMM-CCS experiment successfully detected the small anomalies of bottom water pH caused by the released CO_2 gas, despite the gas release rates being well below what may be tolerated from CCS reservoirs. For this study an ROV was chosen as the monitoring platform as it offered the precise spatial control required for avoiding seabed infrastructure, such as landers and allowed for a detailed study of the CO_2 plume. Nevertheless, the methods developed and described in this work can be applied to other monitoring scenarios and other autonomous platforms such as AUVs. The sensors have different benefits and choosing the most appropriate sensor for the vehicle is an important consideration to ensure sensor and vehicle pairing can increase the potential for leak detection. A summary of the benefits of each sensor is provided in Table 3.

It is essential to consider the velocity of the vehicle relative to the

sensors sampling time to ensure that there would be sufficient spatial resolution to detect a plume. When planning to detect or map a plume it is also key to consider the local hydrodynamics and plume characteristics to ensure that the survey and sensors are appropriate. The most accurate assessment of a plume may be achieved by combining different combinations of sensors and vehicles or landers in multiple packages. For example, to detect and quantify a plume over a large area the optimal surveying technique could be to conduct widespread monitoring utilising an AUV to act as a sniffer. In this case the AUV could be equipped with a fast sampling yet low precision sensor. If the AUV detected a possible plume signal this could trigger a follow up targeted survey, deploying either a lander or ROV equipped with a slower but more accurate sensors to quantify the leak. Alternatively, it may be advantageous to install sensors both fast (e.g. SeaFET™ or optodes) and slow but accurate (e.g. LOC) on a single vehicle and use sensor fusion to generate fast and accurate data.

CRediT authorship contribution statement

Samuel A. Monk: Writing – original draft, Writing – review & editing, Investigation, Formal analysis, Conceptualization, Visualization. **Allison Schaap:** Formal analysis, Investigation, Writing – review & editing, Conceptualization, Data curation, Visualization. **Rudolf Hanz:** Formal analysis, Investigation, Writing – review & editing, Conceptualization, Data curation, Visualization. **Sergey M. Borisov:** Validation, Methodology, Resources. **Socratis Loucaides:** Writing – review & editing, Conceptualization, Supervision. **Martin Arundell:** Methodology, Resources, Supervision. **Stathys Papadimitriou:** Writing – review & editing, Methodology, Resources, Supervision. **John Walk:** Software, Validation, Methodology. **Daisy Tong:** Validation, Methodology. **James Wyatt:** Methodology, Resources. **Matthew Mowlem:** Writing – review & editing, Funding acquisition, Conceptualization.

Declaration of Competing Interest

The authors declare that they have no known competing financial interests or personal relationships that could have appeared to influence the work reported in this paper.

Matt Mowlem is a director, CTO, shareholder and employee of ClearWater Sensors Ltd. that manufacture and sell Lab on Chip chemical sensors utilising intellectual property licensed from the University of Southampton and the National Oceanography Centre. This IP is also used in the sensors described in this paper. Matt maintains employment in the NOC with interactions governed by a detailed conflict of interest policy.

Sam Monk was a student and then postdoc at the University of Southampton and NOC during the development of sensors and the fieldwork described in the paper, but now is a visiting associate at the NOC and is an employee of ClearWater Sensors Ltd.. The majority of this paper was written prior to joining ClearWater Sensors.

those in the Ocean Technology and Engineering Group at NOC responsible for the development and fabrication of the 35 LOC sensors taken on the final cruise, including but not limited to Urska Martincic, Anthony Kenny, Christopher Cardwell, Hannah Wright, Robin Brown, and Kevin Saw.

Supplementary materials

Supplementary material associated with this article can be found, in the online version, at doi:10.1016/j.ijggc.2021.103477.

References

Adams, A.A., Charles, P.T., Veitch, S.P., Hanson, A., Deschamps, J.R., Kusterbeck, A.W., 2013. REMUS100 AUV with an integrated microfluidic system for explosives detection. Anal. Bioanal. Chem. 405, 5171–5178. https://doi.org/10.1007/s00216-013-6853-x.

Alendal, G., 2017. Cost efficient environmental survey paths for detecting continuous tracer discharges. J. Geophys. Res. Ocean. 122, 5458–5467. https://doi.org/10.1002/2016JC012655.

Beaton, A.D., Cardwell, C.L., Thomas, R.S., Sieben, V.J., Legiret, F.E., Waugh, E.M., Statham, P.J., Mowlem, M.C., Morgan, H., 2012. Lab-on-chip measurement of nitrate and nitrite for *in situ* analysis of natural waters. Environ. Sci. Technol. 46, 9548–9556. https://doi.org/10.1021/es300419u.

Beck, A.J., van der Lee, E.M., Eggert, A., Stamer, B., Gledhill, M., Schlosser, C., Achterberg, E.P., 2019. *In Situ* measurements of explosive compound dissolution fluxes from exposed munition material in the Baltic sea. Environ. Sci. Technol. 53, 5652–5660. https://doi.org/10.1021/acs.est.8b06974.

Blackford, J., Alendal, G., Avlesen, H., Brereton, A., Cazenave, P.W., Chen, B., Dewar, M., Holt, J., Phelps, J., 2020. Impact and detectability of hypothetical CCS offshore seep scenarios as an aid to storage assurance and risk assessment. Int. J. Greenh. Gas Control 95, 102949. https://doi.org/10.1016/j.ijggc.2019.102949.

Blackford, J., Artioli, Y., Clark, J., de, Mora, L., 2017. Monitoring of offshore geological carbon storage integrity: Implications of natural variability in the marine system and the assessment of anomaly detection criteria. Int. J. Greenh. Gas Control 64, 99–112. https://doi.org/10.1016/j.ijggc.2017.06.020.

Blackford, J., Bull, J.M., Cevatoglu, M., Connelly, D., Hauton, C., James, R.H., Lichtschlag, A., Stahl, H., Widdicombe, S., Wright, I.C., 2015. Marine base line and monitoring strategies for carbon dioxide capture and storage (CCS). Int. J. Greenh. Gas Control 38, 221–229. https://doi.org/10.1016/j.ijggc.2014.10.004.

Blackford, J., Stahl, H., Bull, J.M., Bergès, B.J.P., Cevatoglu, M., Lichtschlag, A., Connelly, D., James, R.H., Kita, J., Long, D., Naylor, M., Shitashima, K., Smith, D., Taylor, P., Wright, I., Akhurst, M., Chen, B., Gernon, T.M., Hauton, C., Hayashi, M., Kaieda, H., Leighton, T.G., Sato, T., Sayer, M.D.J., Suzumura, M., Tait, K., Vardy, M.E., White, P.R., Widdicombe, S., 2014. Detection and impacts of leakage from sub-seafloor deep geological carbon dioxide storage. Nat. Clim. Change 4, 1011–1016. https://doi.org/10.1038/nclimate2381.

Bockmon, E.E., Dickson, A.G., 2015. An inter-laboratory comparison assessing the quality of seawater carbon dioxide measurements. Mar. Chem. 171, 36–43. https://doi.org/10.1016/j.marchem.2015.02.002.

Bresnahan, P.J., Martz, T.R., Takeshita, Y., Johnson, K.S., LaShomb, M., 2014. Best practices for autonomous measurement of seawater pH with the Honeywell durafet. Methods Oceanogr. 9, 44–60. https://doi.org/10.1016/j.mio.2014.08.003.

Bresnahan, P.J., Takeshita, Y., Wirth, T., Martz, T.R., Cyronak, T., Albright, R., Wolfe, K., Warren, J.K., Mertz, K., 2021. Autonomous *in situ* calibration of ion-sensitive field effect transistor pH sensors. Limnol. Oceanogr. Methods 19, 132–144. https://doi.org/10.1002/lom3.10410.

Bushinsky, S.M., Takeshita, Y., Williams, N.L., 2019. Observing changes in ocean carbonate chemistry: our autonomous future. Curr. Clim. Change Rep. 5, 207–220. https://doi.org/10.1007/s40641-019-00129-8.

Cevatoglu, M., Bull, J.M., Vardy, M.E., Gernon, T.M., Wright, I.C., Long, D., 2015. Gas migration pathways, controlling mechanisms and changes in sediment acoustic properties observed in a controlled sub-seabed CO_2 release experiment. Int. J. Greenh. Gas Control 38, 26–43. https://doi.org/10.1016/j.ijggc.2015.03.005.

Chai, F., Johnson, K.S., Claustre, H., Xing, X., Wang, Y., Boss, E., Riser, S., Fennel, K., Schofield, O., Sutton, A., 2020. Monitoring ocean biogeochemistry with autonomous platforms. Nat. Rev. Earth Environ. 1, 315–326. https://doi.org/10.1038/s43017-020-0053-y.

Choyekh, M., Kato, N., Yamaguchi, Y., Dewantara, R., Chiba, H., Senga, H., Yoshie, M., Tanaka, T., Kobayashi, E., Short, T., 2017. Development and operation of underwater robot for autonomous tracking and monitoring of subsea plumes after oil spill and gas leak from seabed and analyses of measured data. In: Kato, N. (Ed.), Applications to Marine Disaster Prevention: Spilled Oil and Gas Tracking Buoy System, ed. Springer Japan, Tokyo, pp. 17–93.

Clayton, T.D., Byrne, R.H., 1993. Spectrophotometric seawater pH measurements: total hydrogen ion concentration scale calibration of m-cresol purple and at-sea results. Deep. Res. Part I 40, 2115–2129. https://doi.org/10.1016/0967-0637(93)90048-8.

Clinton-Bailey, G.S., Grand, M.M., Beaton, A.D., Nightingale, A.M., Owsianka, D.R., Slavik, G.J., Connelly, D.P., Cardwell, C.L., Mowlem, M.C., 2017. A lab-on-chip analyzer for *in Situ* measurement of soluble reactive phosphate: improved phosphate blue assay and application to fluvial monitoring. Environ. Sci. Technol. 51, 9989–9995. https://doi.org/10.1021/acs.est.7b01581.

Connelly, D.P., 2019. RRS James cook cruise JC108 25 April –30 May 2019. Strategies for the Environmental Monitoring of Marine Carbon Capture and Storage. STEMM-CCS.

Connelly, D.P., Copley, J.T., Murton, B.J., Stansfield, K., Tyler, P.A., German, C.R., Van Dover, C.L., Amon, D., Furlong, M., Grindlay, N., Hayman, N., Hühnerbach, V., Judge, M., Le Bas, T., McPhail, S., Meier, A., Nakamura, K.I., Nye, V., Pebody, M., Pedersen, R.B., Plouviez, S., Sands, C., Searle, R.C., Stevenson, P., Taws, S., Wilcox, S., 2012. Hydrothermal vent fields and chemosynthetic biota on the world's deepest seafloor spreading centre. Nat. Commun. 3 https://doi.org/10.1038/ncomms1636.

Dean, M., Blackford, J., Connelly, D., Hines, R., 2020. Insights and guidance for offshore CO_2 storage monitoring based on the QICS, ETI MMV, and STEMM-CCS projects. Int. J. Greenh. Gas Control 100, 103120. https://doi.org/10.1016/j.ijggc.2020.103120.

Dean, M., Tucker, O., 2017. A risk-based framework for measurement, monitoring and verification (MMV) of the goldeneye storage complex for the Peterhead CCS project, UK. Int. J. Greenh. Gas Control 61, 1–15. https://doi.org/10.1016/j.ijggc.2017.03.014.

Dewar, M., Sellami, N., Chen, B., 2015. Dynamics of rising CO_2 bubble plumes in the QICS field experiment. Part 2 - modelling. Int. J. Greenh. Gas Control 38, 52–63. https://doi.org/10.1016/j.ijggc.2014.11.003.

Dickson, A.G., 1990. Thermodynamics of the dissociation of boric acid in potassium chloride solutions from 273.15 to 318.15 K. J. Chem. Eng. Data 35, 253–257. https://doi.org/10.1021/je00061a009.

Dickson, A.G., 1981. An exact definition of total alkalinity and a procedure for the estimation of alkalinity and total inorganic carbon from titration data. Deep Sea Res. Part A Oceanogr. Res. Pap. 28, 609–623. https://doi.org/10.1016/0198-0149(81)90121-7.

Dickson, A.G., Goyet, C., 1994. Handbook of methods for the analysis of the various parameters of the carbon dioxide system in sea water, version 2. 10.2172/10107773.

Dickson, A.G., Millero, F.J., 1987. A comparison of the equilibrium constants for the dissociation of carbonic acid in seawater media. Deep Sea Res. Part A, Oceanogr. Res. Pap. 34, 1733–1743. https://doi.org/10.1016/0198-0149(87)90021-5.

Dickson, A.G., Sabine, C.L., Christian, J.R., 2007. Guide to best practices for ocean CO_2 measurements. PICES Spec. Publ. 3, p191. https://doi.org/10.1159/000331784.

Dixon, T., Romanak, K.D., 2015. Improving monitoring protocols for CO_2 geological storage with technical advances in CO_2 attribution monitoring. Int. J. Greenh. Gas Control 41, 29–40. https://doi.org/10.1016/j.ijggc.2015.05.029.

Dock, M.L., Harper, R.J., Knobbe, E., 2010. Combined pre-Concentration and Real-Time *In-Situ* Chemical Detection of Explosives in the Marine Environment. Ocean Sensing and Monitoring II. International Society for Optics and Photonics, p. 76780U. https://doi.org/10.1117/12.850727.

Esposito, M., Martinez-Cabanas, M., Achterberg, E.P., 2019. Hydrochemistry and carbonate chemistry measured on water bottle samples during POSEIDON cruise POS527. 10.1594/PANGAEA.907809.

Esposito, M., Martínez-Cabanas, M., Connelly, D.P., Jasinski, D., Linke, P., Schmidt, M., Achterberg, E.P., 2021. Water column baseline assessment for offshore carbon dioxide capture and Storage (CCS) sites: analysis of field data from the Goldeneye storage complex area [SUBMITTED]. Int. J. Greenh. Gas Control.

Flohr, A., Schaap, A., Achterberg, E.P., Alendal, G., Arundell, M., Berndt, C., Blackford, J., Böttner, C., Borisov, S.M., Brown, R., Bull, J.M., Carter, L., Chen, B., Dale, A.W., de Beer, D., Dean, M., Deusner, C., Dewar, M., Durden, J.M., Elsen, S., Esposito, M., Faggetter, M., Fischer, J.P., Gana, A., Gros, J., Haeckel, M., Hanz, R., Holtappels, M., Hosking, B., Huvenne, V.A.I., James, R.H., Koopmans, D., Kossel, E., Leighton, T.G., Li, J., Lichtschlag, A., Linke, P., Loucaides, S., Martínez-Cabanas, M., Matter, J.M., Mesher, T., Monk, S., Mowlem, M., Oleynik, A., Papadimitriou, S., Paxton, D., Pearce, C.R., Peel, K., Roche, B., Ruhl, H.A., Saleem, U., Sands, C., Saw, K., Schmidt, M., Sommer, S., Strong, J.A., Triest, J., Ungerböck, B., Walk, J., White, P., Widdicombe, S., Wilson, R.E., Wright, H., Wyatt, J., Connelly, D., 2021. Towards improved monitoring of offshore carbon storage: a real-world field experiment detecting a controlled sub-seafloor CO_2 release. Int. J. Greenh. Gas Control 106. https://doi.org/10.1016/j.ijggc.2020.103237.

Fritzsche, E., Staudinger, C., Fischer, J.P., Thar, R., Jannasch, H.W., Plant, J.N., Blum, M., Massion, G., Thomas, H., Hoech, J., Johnson, K.S., Borisov, S.M., Klimant, I., 2018. A validation and comparison study of new, compact, versatile optodes for oxygen, pH and carbon dioxide in marine environments. Mar. Chem. 207, 63–76. https://doi.org/10.1016/j.marchem.2018.10.009.

Furlong, M.E., Paxton, D., Stevenson, P., Pebody, M., McPhail, S.D., Perrett, J., 2012. Autosub long range: a long range deep diving AUV for ocean monitoring. In: Proceeding of the IEEE/OES Autonomous Underwater Vehicles AUV. https://doi.org/10.1109/AUV.2012.6380737.

German, C.R., Jakuba, M.V., Kinsey, J.C., Partan, J., Suman, S., Belani, A., Yoerger, D.R., 2012. A long term vision for long-range ship-free deep ocean operations: persistent presence through coordination of autonomous surface vehicles and autonomous underwater vehicles. In: Proceeding of the IEEE/OES Autonomous Underwater Vehicles AUV. https://doi.org/10.1109/AUV.2012.6380753.

Grand, M.M., Clinton-Bailey, G.S., Beaton, A.D., Schaap, A.M., Johengen, T.H., Tamburri, M.N., Connelly, D.P., Mowlem, M.C., Achterberg, E.P., 2017. A lab-on-chip phosphate analyzer for long-term *in situ* monitoring at fixed observatories: optimization and performance evaluation in estuarine and oligotrophic coastal waters. Front. Mar. Sci. 4, 1–16. https://doi.org/10.3389/fmars.2017.00255.

Gros, J., Schmidt, M., Dale, A.W., Linke, P., Vielstädte, L., Bigalke, N., Haeckel, M., Wallmann, K., Sommer, S., 2019. Simulating and quantifying multiple natural subsea CO_2 seeps at panarea Island (Aeolian Islands, Italy) as a proxy for potential leakage from subseabed carbon storage sites. Environ. Sci. Technol. 53, 10258–10268. https://doi.org/10.1021/acs.est.9b02131.

Guerrero-González, A., García-Córdova, F., Ortiz, F.J., Alonso, D., Gilabert, J., 2016. A multirobot platform based on autonomous surface and underwater vehicles with bio-inspired neurocontrollers for long-term oil spills monitoring. Auton. Robots 40, 1321–1342. https://doi.org/10.1007/s10514-016-9602-0.

Hemming, M.P., Kaiser, J., Heywood, K.J., Bakker, D.C.E., Boutin, J., Shitashima, K., Lee, G., Legge, O., Onken, R., 2017. Measuring pH variability using an experimental sensor on an underwater glider. Ocean Sci. 13, 427–442. https://doi.org/10.5194/os-13-427-2017.

Hwang, J., Bose, N., Fan, S., 2019. AUV adaptive sampling methods: a review. Appl. Sci. 9 https://doi.org/10.3390/app9153145.

IEA Greenhouse Gas R&D Programme, D.R.D., 2008. Assessment of sub sea ecosystem impacts 1–266.

IPCC, 2005. IPCC Special Report on Carbon Dioxide Capture and Storage. Prepared by Working Group III of the Intergovernmental Panel on Climate Change. Cambridge University Press, Cambridge.

IPIECA, IOGP, 2014. Capabilities and uses of sensor-equipped ocean vehicles for subsea and surface detection and tracking of oil spills, IPIECA/IOGP oil spill response JIP.

Jansen, H.M., Broch, O.J., Bannister, R., Cranford, P., Handå, A., Husa, V., Jiang, Z., Strohmeier, T., Strand, 2018. Spatio-temporal dynamics in the dissolved nutrient waste plume from Norwegian salmon cage aquaculture. Aquac. Environ. Interact. 10, 385–399. https://doi.org/10.3354/AEI00276.

Johnson, K.S., Jannasch, H.W., Coletti, L.J., Elrod, V.A., Martz, T.R., Takeshita, Y., Carlson, R.J., Connery, J.G., 2016. Deep-Sea DuraFET: a pressure tolerant pH sensor designed for global sensor networks. Anal. Chem. 88, 3249–3256. https://doi.org/10.1021/acs.analchem.5b04653.

Jones, B., Teel, E., Seegers, B., Ragan, M., 2015. Observing, monitoring and evaluating the effects of discharge plumes in coastal regions. In: Missimer, T.M., Jones, B., Maliva, R.G. (Eds.), Environmental Science and Engineering (Subseries: Environmental Science), Eds. Environmental Science and Engineering. Springer International Publishing, pp. 521–538. https://doi.org/10.1007/978-3-319-13203-7_22.

Kato, N., Choyekh, M., Dewantara, R., Senga, H., Chiba, H., Kobayashi, E., Yoshie, M., Tanaka, T., Short, T., 2017. An autonomous underwater robot for tracking and monitoring of subsea plumes after oil spills and gas leaks from seafloor. J. Loss Prev. Process Ind. 50, 386–396. https://doi.org/10.1016/j.jlp.2017.03.006.

Ketzer, J.M., Machado, C.X., Rockett, G.C., Iglesias, R.S., 2015. *(Eds.)* Brazilian Atlas of CO_2 Capture and Geological Storage. EdiPUCRS, Porto Alegre, Brazil.

Kivenson, V., Lemkau, K.L., Pizarro, O., Yoerger, D.R., Kaiser, C., Nelson, R.K., Carmichael, C., Paul, B.G., Reddy, C.M., Valentine, D.L., 2019. Ocean dumping of containerized DDT waste was a sloppy process. Environ. Sci. Technol. 53, 2971–2980. https://doi.org/10.1021/acs.est.8b05859.

Klimant, I., Huber, C., Liebsch, G., Neurauter, G., Stangelmayer, A., Wolfbeis, O.S., 2001. Dual lifetime referencing (DLR) — a new scheme for converting fluorescence intensity into a frequency-domain or time-domain information BT - New Trends in Fluorescence Spectroscopy: Applications to Chemical and Life Sciences, in: Valeur, B., Brochon, J.C. (Eds.), Springer Berlin Heidelberg, Berlin, Heidelberg, pp. 257–274. 10.1007/978-3-642-56853-4_13.

Lewis, E., Wallace, D.W.R., 1998. Program Developed for CO_2 System Calculations (Carbon Dioxide Information Analysis Center. Oak Ridge National Laboratory, US Department of Energy, Oak Ridge, TN. ORNL/CDIAC-105.

Lichtschlag, A., James, R.H., Stahl, H., Connelly, D., 2015. Effect of a controlled sub-seabed release of CO_2 on the biogeochemistry of shallow marine sediments, their pore waters, and the overlying water column. Int. J. Greenh. Gas Control 38, 80–92. https://doi.org/10.1016/j.ijggc.2014.10.008.

Mac Dowell, N., Fennell, P.S., Shah, N., Maitland, G.C., 2017. The role of CO_2 capture and utilization in mitigating climate change. Nat. Clim. Change 7, 243–249. https://doi.org/10.1038/nclimate3231.

Martz, T.R., Connery, J.G., Johnson, K.S., 2010. Testing the Honeywell Durafet® for seawater pH applications. Limnol. Oceanogr. Methods 8, 172–184. https://doi.org/10.4319/lom.2010.8.172.

McLaughlin, K., Dickson, A., Weisberg, S.B., Coale, K., Elrod, V., Hunter, C., Johnson, K.S., Kram, S., Kudela, R., Martz, T., Negrey, K., Passow, U., Shaughnessy, F., Smith, J.E., Tadesse, D., Washburn, L., Weis, K.R., 2017. An evaluation of ISFET sensors for coastal pH monitoring applications. Reg. Stud. Mar. Sci. 12, 11–18. https://doi.org/10.1016/j.rsma.2017.02.008.

McStay, D., McIlroy, J., Forte, A., Lunney, F., Greenway, T., Thabeth, K., Dean, G., 2005. A new tool for the rapid remote detection of leaks from subsea pipelines during remotely operated vehicle inspections. J. Opt. A Pure Appl. Opt. 7, S346–S351. https://doi.org/10.1088/1464-4258/7/6/014.

Mehrbach, C., Culberson, C.H., Hawley, J.E., Pytkowicx, R.M., 1973. Measurement of the apparent dissociation constants of carbonic acid in seawater At atmospheric

pressure. Limnol. Oceanogr. 18, 897–907. https://doi.org/10.4319/lo.1973.18.6.0897.

Millero, F.J., 2007. The marine inorganic carbon cycle. Chem. Rev. 107, 308–341. https://doi.org/10.1021/cr0503557.

Moodie, D., Costello, L., McStay, D, D, M., Costello, L., McStay, D., 2010. Optoelectronic leak detection system for monitoring subsea structures. Optical Sensing and Detection. International Society for Optics and Photonics, p. 77260N. https://doi.org/10.1117/12.854483.

Rérolle, V., Floquet, C.F.A.A., Mowlem, M.C., Connelly, D.P., Achterberg, E.P., Bellerby, R.R.G.J., 2012. Seawater-pH measurements for ocean-acidification observations. TrAC Trends Anal. Chem. 40, 146–157. https://doi.org/10.1016/j.trac.2012.07.016.

Roemmich, D., Alford, M.H., Claustre, H., Johnson, K.S., King, B., Moum, J., Oke, P.R., Owens, W.B., Pouliquen, S., Purkey, S., Scanderbeg, M., Suga, T., Wijffels, S.E., Zilberman, N., Bakker, D., Baringer, M.O., Belbeoch, M., Bittig, H.C., Boss, E., Calil, P., Carse, F., Carval, T., Chai, F., Conchubhair, D.O., D'Ortenzio, F., Dall'Olmo, G., Desbruyères, D., Fennel, K., Fer, I., Ferrari, R., Forget, G., Freeland, H., Fujiki, T., Gehlen, M., Greenan, B., Hallberg, R., Hibiya, T., Hosoda, S., Jayne, S., Jochum, M., Johnson, G.C., Kang, K.R., Kolodziejczyk, N., Koertzinger, A., Le Traon, P.Y., Lenn, Y.D., Maze, G., Mork, K.A., Morris, T., Nagai, T., Nash, J., Garabato, A.N., Olsen, A., Pattabhi, R.R., Prakash, S., Riser, S., Schmechtig, C., Shroyer, E., Sterl, A., Sutton, P., Talley, L., Tanhua, T., Thierry, V., Thomalla, S., Toole, J., Troisi, A., Trull, T., Turton, J.D., Velez-Belchi, P.J., Walczowski, W., Wang, H., Wanninkhof, R., Waterhouse, A., Watson, A., Wilson, C., Wong, A.P., Xu, J., Yasuda, I., 2019. On the future of Argo: a global, full-depth, multi-disciplinary array. Front. Mar. Sci. 6, 1–28. https://doi.org/10.3389/fmars.2019.00439.

Rogowski, P., Terrill, E., Otero, M., Hazard, L., Middleton, W., 2012. Mapping ocean outfall plumes and their mixing using autonomous underwater vehicles. J. Geophys. Res. Ocean. 117 https://doi.org/10.1029/2011JC007804.

Saba, G.K., Wright-Fairbanks, E., Chen, B., Cai, W.J., Barnard, A.H., Jones, C.P., Branham, C.W., Wang, K., Miles, T., 2019. The development and validation of a Profiling glider deep ISFET-based pH sensor for high resolution observations of coastal and ocean acidification. Front. Mar. Sci. 6, 1–17. https://doi.org/10.3389/fmars.2019.00664.

Schaap, A., Koopmans, D., Holtappels, M., Dewar, M., Arundell, M., Papadimitriou, S., Hanz, R., Monk, S., Mowlem, M., Loucaides, S., 2021. Quantification of a subsea CO_2 release with lab-on-chip sensors measuring benthic gradients. Int. J. Greenh. Gas Control.

Schmidt, M., Linke, P., Sommer, S., Esser, D., Cherednichenko, S., 2014. Natural CO_2 seeps offshore panarea: a test site for subsea CO_2 leak detection technology. Mar. Technol. Soc. J. 49, 19–30. https://doi.org/10.4031/MTSJ.49.1.3.

Schrag, D.P., 2009. Storage of carbon dioxide in offshore sediments. Science 325 (80), 1658–1659. https://doi.org/10.1126/science.1175750.

Shukla, A., Karki, H., 2016. Application of robotics in offshore oil and gas industry-a review Part II. Rob. Auton. Syst. 75, 508–524. https://doi.org/10.1016/j.robot.2015.09.013.

Singh, H., Eustice, R., Roman, C., Pizarro, O., 2002. The SeaBED AUV - a platform for high resolution imaging. Unmanned Underw. Veh. Showc. Conf. Exibit.

Spearman, J., Taylor, J., Crossouard, N., Cooper, A., Turnbull, M., Manning, A., Lee, M., Murton, B., 2020. Measurement and modelling of deep sea sediment plumes and implications for deep sea mining. Sci. Rep. 10, 1–14. https://doi.org/10.1038/s41598-020-61837-y.

Spence, B., Horan, D., Tucker, O., 2014. The peterhead-goldeneye gas post-combustion CCS project. Energy Proced. 63, 6258–6266. https://doi.org/10.1016/j.egypro.2014.11.657.

Staudinger, C., Strobl, M., Breininger, J., Klimant, I., Borisov, S.M., 2019. Fast and stable optical pH sensor materials for oceanographic applications. Sens. Actuators B Chem. 282, 204–217. https://doi.org/10.1016/j.snb.2018.11.048.

Staudinger, C., Strobl, M., Fischer, J.P., Thar, R., Mayr, T., Aigner, D., Müller, B.J., Müller, B., Lehner, P., Mistlberger, G., Fritzsche, E., Ehgartner, J., Zach, P.W., Clarke, J.S., Geißler, F., Mutzberg, A., Müller, J.D., Achterberg, E.P., Borisov, S.M., Klimant, I., 2018. A versatile optode system for oxygen, carbon dioxide, and pH measurements in seawater with integrated battery and logger. Limnol. Oceanogr. Methods 16, 459–473. https://doi.org/10.1002/lom3.10260.

Takeshita, Y., Jones, B.D., Johnson, K.S., Chavez, F.P., Rudnick, D.L., Blum, M., Conner, K., Jensen, S., Long, J.S., Maughan, T., Mertz, K.L., Sherman, J.T., Warren, J.K., 2021. Accurate pH and O_2 measurements from spray underwater gliders. J. Atmos. Ocean. Technol. 38, 181–195. https://doi.org/10.1175/JTECH-D-20-0095.1.

Tamburri, M., Johengen, T., Smith, G.J., Schar, D., Atkinson, M., Purcell, H., Loewensteiner, D., Epperson, Z., 2015. Performance verification statement for the satlantic SeaFET pH sensor. Maryland, USA. https://www.act-us.info/Download/Evaluations/pH/Satlantic/files/assets/common/downloads/publication.pdf.

UNFCCC. Conference of the Parties (COP), 2015. Adoption of the Paris agreement. In: Proceeding of the President Climate Change Conference in Paris, p. 32. COP 21 21932FCCC/CP/2015/L.9/Rev.1.

Uppström, L.R., 1974. The boron/chlorinity ratio of deep-sea water from the Pacific Ocean. Deep. Res. Oceanogr. Abstr. 21, 161–162. https://doi.org/10.1016/0011-7471(74)90074-6.

van Heuven, S., Pierrot, D., Rae, J.W.B., Lewis, E., Wallace, D.W.R., 2011. MATLAB Program Developed for CO_2 System Calculations. ORNL/CDIAC-105b. ORNL/CDIAC-105b. Carbon Dioxide Information Analysis Center, Oak Ridge National Laboratory U.S. Department Energy, Oak Ridge, Tennessee. https://doi.org/10.3334/CDIAC/otg.CO2SYS_MATLAB_v1.1.

Vincent, A.G., Pascal, R.W., Beaton, A.D., Walk, J., Hopkins, J.E., Woodward, E.M.S., Mowlem, M., Lohan, M.C., 2018. Nitrate drawdown during a shelf sea spring bloom

revealed using a novel microfluidic *in situ* chemical sensor deployed within an autonomous underwater glider. Mar. Chem. 205, 29–36. https://doi.org/10.1016/j.marchem.2018.07.005.

Wallmann, K., Haeckel, M., Linke, P., Haffert, L., Schmidt, M., Buenz, S., James, R., Hauton, C., Tsimplis, M., Widdicombe, S., Blackford, J., Queiros, A.M., Connelly, D., Lichtschlag, A., Dewar, M., Chen, B., Baumberger, T., Beaubin, S., Vercelli, S., Proelss, A., Wildenborg, T., Mikunda, T., Nepveu, M., Maynard, C., Finnerty, S., Flach, T., Ahmed, N., Ulfsnes, A., Brooks, L., Moskeland, T., Purcell, M., 2015. Best practice guidance for environmental risk assessment for offshore CO2 geological storage. 10.3289/ECO2_D14.1.

Wang, Z.A., Moustahfid, H., Mueller, A.V., Michel, A.P.M., Mowlem, M., Glazer, B.T., Mooney, T.A., Michaels, W., McQuillan, J.S., Robidart, J.C., Churchill, J., Sourisseau, M., Daniel, A., Schaap, A., Monk, S., Friedman, K., Brehmer, P., 2019. Advancing observation of ocean biogeochemistry, biology, and ecosystems with cost-effective *in situ* sensing technologies. Front. Mar. Sci. 6, 1–22. https://doi.org/10.3389/fmars.2019.00519.

Williams, R.G., Follows, M.J., 2011. Ocean Dynamics and the Carbon Cycle, 1st ed. Cambridge Unvserity Press.

Wolf-Gladrow, D.A., Zeebe, R.E., Klaas, C., Körtzinger, A., Dickson, A.G., 2007. Total alkalinity: the explicit conservative expression and its application to biogeochemical processes. Mar. Chem. 106, 287–300. https://doi.org/10.1016/j.marchem.2007.01.006.

Yin, T., Papadimitriou, S., Rérolle, V.M.C., Arundell, M., Cardwell, C.L., Walk, J., Palmer, M.R., Fowell, S., Schaap, A., Mowlem, M.C., Loucaides1, S., 2021. A novel lab-on-chip spectrophotometric pH sensor for autonomous *in situ* seawater measurements to 6000 m depth on stationary and moving observing platforms (in press). Environ. Sci. Technol.

Yoerger, D., Bradley, A., Jakuba, M., German, C., Shank, T., Tivey, M., 2007. Autonomous and remotely operated vehicle technology for hydrothermal vent discovery, exploration, and sampling. Oceanography 20, 152–161. https://doi.org/10.5670/oceanog.2007.89.